Intraseasonal Teleconnection between the Summer Eurasian Wave Train and the Indian Monsoon*

QINGHUA DING AND BIN WANG+

Department of Meteorology, School of Ocean and Earth Science and Technology, University of Hawaii at Manoa, Honolulu, Hawaii

(Manuscript received 30 December 2005, in final form 29 November 2006)

ABSTRACT

This study investigated the most recurrent coupled pattern of intraseasonal variability between midlatitude circulation and the Indian summer monsoon (ISM). The leading singular vector decomposition (SVD) pattern reveals a significant, coupled intraseasonal variation between a Rossby wave train across the Eurasian continent and the summer monsoon convection in northwestern India and Pakistan (hereafter referred to as NISM). The wave train associated with an active phase of NISM rainfall displays two high pressure anomalies, one located over central Asia and the other over northeastern Asia. They are accompanied by increased rainfall over the western Siberia plain and northern China and decreased rainfall over the eastern Mediterranean Sea and southern Japan. The circulation of the wave train shows a barotropic structure everywhere except the anomalous central Asian high, located to the northwest of India, where a heat-induced baroclinic circulation structure dominates. The time-lagged SVD analysis shows that the midlatitude wave train originates from the northeastern Atlantic and traverses Europe to central Asia. The wave train enhances the upper-level high pressure and reinforces the convection over the NISM region; meanwhile, it propagates farther toward East Asia along the waveguide provided by the westerly jet. After an outbreak of NISM convection, the anomalous central Asian high retreats westward. Composite analysis suggests a coupling between the central Asian high and the convective fluctuation in the NISM. The significance of the midlatitude–ISM interaction is also revealed by the close resemblance between the individual empirical orthogonal functions and the coupled (SVD) modes of the midlatitude circulation and the ISM.

It is hypothesized that the eastward and southward propagation of the wave train originating from the northeastern Atlantic contributes to the intraseasonal variability in the NISM by changing the intensity of the monsoonal easterly vertical shear and its associated moist dynamic instability. On the other hand, the rainfall variations over the NISM reinforce the variations of the central Asian high through the "monsoon–desert" mechanism, thus reenergizing the downstream propagation of the wave train. The coupling between the Eurasian wave train and NISM may be instrumental for understanding their interaction and can provide a way to predict the intraseasonal variations of the Indian summer monsoon and East Asian summer monsoon.

1. Introduction

The "active" and "break" cycles of the Indian summer monsoon (ISM) rainfall manifest the boreal summer monsoon intraseasonal variability (Webster et al. 1998). The periodicity of intraseasonal oscillations (ISOs) over India shows a wide time-scale range, from 10 to 60 days, with significant double spectral peaks at 30–60 days and at 10–20 days (Krishnamurti and Bhalme 1976; Murakami et al. 1984; Annamalai and Slingo 2001). Both the northward-propagating 30–60-day ISO events and the westward-propagating 10–20-day ISO events are the main rainfall-producing mechanisms for the ISM. The majority of 30–60-day oscilla-

* School of Ocean and Earth Science and Technology Contribution Number 7033 and International Pacific Research Center Contribution Number 427.

+ Additional affiliation: International Pacific Research Center, School of Ocean and Earth Science and Technology, University of Hawaii at Manoa, Honolulu, Hawaii, and Marine Environmental College, Ocean University of China, Qingdao, China.

Corresponding author address: Mr. Qinghua Ding, Department of Meteorology, School of Ocean and Earth Science and Technology, University of Hawaii at Manoa, 2525 Correa Rd., Honolulu, HI 96822.
E-mail: qinghua@hawaii.edu

DOI: 10.1175/JCLI4221.1

tion events that influence the ISM originate from the equatorial Indian Ocean (Yasunari 1979, 1980; Sikka and Gadgil 1980; Krishnamurti and Subrahmanyam 1982; Hartmann and Michelson 1989; Wang and Rui 1990). The physical mechanisms that give rise to the northward propagation of the 30–60-day oscillation have been attributed to convection–radiation–surface heat flux feedback (Webster 1983; Goswami and Shukla 1984), the effects of easterly vertical shear on moist Rossby waves (Wang and Xie 1997; Jiang et al. 2004; Wang 2005), and the air–sea interaction (Kemball-Cook and Wang 2001; Fu et al. 2003).

However, to what extent the ISM interacts with the midlatitude circulation on intraseasonal time scales has not been firmly established, although a few studies have noted the influence of midlatitude synoptic disturbance on the ISM (Keshavamurty and Rao 1992) and the linkage of an ISM break with weakening midlatitude zonal flow and the southward-penetrating midtropospheric westerly trough (Ramaswamy 1962). Based on case studies, Raman and Rao (1981) noted the existence of two upper-tropospheric blocking ridges situated over the north Caspian Sea and eastern Siberia during severe drought years of the ISM; the evolution of these blocking ridges and the corresponding wave activity were closely related to monsoon breaks. However, Kripalani et al. (1997) considered the ridge to the northwest of India as a sign of the active monsoon over northern and central India. Using 3 yr of data (1986, 1993, and 1998), Fujinami and Yasunari (2004) found that the 7–20-day convective variability over the Tibetan Plateau is associated with a wave train propagating from North Africa to Japan, which appears to influence convective variations over the plateau and surrounding regions. A conventional notion is that the continent–ocean thermal contrast is a dominant factor driving the ISM; thus, any midlatitude system that is able to effectively modulate the thermal contrast can influence the monsoon intensity (Tao and Chen 1987; Kripalani et al. 1997; Ding and Sikka 2005). On the other hand, a burst of deep convection over India could in turn affect the midlatitude flow farther downstream through the excitation of Rossby wave trains (Yasunari 1986; Annamalai and Slingo 2001; Wang et al. 2001; Ding and Wang 2005).

The previous findings led us to speculate that there exists a possible mutual interplay between the midlatitude systems and the Indian monsoon. The present observational analysis is devoted to a comprehensive examination of the boreal summer tropical–extratropical interaction on the intraseasonal time scale. Major questions addressed in this paper include the following: 1) is there any significant, recurrent coupled pattern between the midlatitude circulation and ISM on the intraseasonal time scale? and 2) if the answer is yes, then how does this coupled mode evolve with time and influence the rainfall variation over India and other areas? By putting together all pieces of observed evidence, we aimed to formulate a new hypothesis for the intraseasonal interaction between the boreal summer midlatitude circulation and the Indian monsoon.

2. Data and analysis procedures

a. Data

The major dataset used in this work was the daily mean National Centers for Environmental Prediction–National Center for Atmospheric Research (NCEP–NCAR) reanalysis data on a 2.5° by 2.5° grid and at the standard pressure levels. Because of the high elevation of the Tibetan Plateau, the geopotential height in 200 hPa was used to represent midlatitude flow over Eurasia. Daily averages of outgoing longwave radiation (OLR) data on a 2.5° square grid, obtained through the National Oceanic and Atmospheric Administration satellite, were used as a proxy for large-scale convective activity over the tropical and subtropical regions (Liebmann and Smith 1996). To verify the ability of OLR to measure rainfall variability over the Indian subcontinent, the gridded (2.5° × 2.5°) precipitation pentad data from the Global Precipitation Climatology Project (GPCP) were compared with the OLR field. The GPCP data were interpolated from pentad means to daily values. The correlation between 25 summer (1979–2003) daily OLR and GPCP data shows a high correlation coefficient (0.8) over the ocean and a reduced correlation coefficient (0.6) over the Indian subcontinent (figures not shown). This suggests that OLR can be used as an indicator of the large-scale convection and precipitation over the ISM region with a daily resolution.

b. Time filter scheme

Unlike previous studies, which focus mostly on individual years or case studies, we used a dataset covering 25 consecutive boreal summers from 1979 to 2003 to determine possible links between the northern summer midlatitude flows and the ISM rainfall. The summer season was defined as a 122-day period from 1 June to 30 September. To examine the fluctuations in a broad range of frequencies on the intraseasonal time scale, a three-step temporal filtering scheme was applied to daily data to remove long-term variability and trends while preserving intraseasonal variability as much as possible. First, a 25-summer averaged, least squares fitting parabola was removed from the unfiltered data to

remove the climatological seasonal cycle. Then, the mean of each season was removed in order to eliminate interannual variability. Finally, a five-day running mean time filter was applied to the daily data to eliminate synoptic variability. All data used in the remainder of this study were filtered by these three-step processes.

c. Significance test

With the filtered data, all meteorological variables involve high autocorrelations between consecutive daily values. Thus, the degree of freedom should be much less than with the original sample size (2950 daily values). Using Chen's (1982) method, the degrees of freedom for each variable at each grid within the Eurasian domain (0°–90°N, 40°W–180°) were calculated. The smallest degree of freedom was found to be about 450. For simplicity, we have assumed that the degrees of freedom for each variable are 450 at every grid point for the purpose of a statistical significance test. With this degree of freedom, a correlation coefficient with a magnitude greater than 0.1 is statistically significant at the 95% confidence level.

In addition, the significance of correlation coefficients was retested through the 1000 times Monte Carlo simulation procedure (Wilks 1995; Livezey and Chen 1983). In all cases studied here, we found that the confidence level determined by this Monte Carlo technique was much less than the correlation coefficient value of 0.1 obtained from the first method. Thus, in the following sections, the correlations with absolute values of coefficients exceeding 0.1 are shown, and they are regarded as significantly different from zero.

d. Statistical tools: Singular vector decomposition

The main statistical tools utilized in this study include singular vector decomposition (SVD) analysis, empirical orthogonal function (EOF) analysis, and composite analysis. The SVD analysis was used to capture the most dominant coupling mode between the midlatitude circulation and the ISM. To reveal the evolution of this coupled tropical–extratropical mode, a time-lagged SVD analysis was further used. This method is the same as SVD analysis except that a time lag between the two fields was introduced. The advantage of this method is that it captures the optimum lead–lag relationship between the two fields examined. A complementary composite method was used to facilitate the discussion of several mechanisms. To clarify whether the coupled SVD mode is significant in its respective field, an EOF analysis was used to extract the leading EOF modes of individual fields, which provided for a direct comparison with the coupled SVD patterns.

A detailed description of the SVD method and its application can be found in Bretherton et al. (1992) and Wallace et al. (1992). Briefly, the SVD of the temporal covariance matrix between two geophysical fields is an extension of rectangular matrices in the diagonalization procedure of a square symmetric matrix. Based on the time series of the two different fields, a covariance matrix can be formed and expanded to pairs of singular vectors (right and left), describing the spatial patterns of the two fields. The associated singular value represents the squared covariance fraction (SCF) and indicates the percentage of the total squared covariance explained by the corresponding singular vectors. Thus, the SCF also measures the relative importance of that pair of vectors in the relationship to the two fields. In addition, the expansion coefficient obtained by projecting the singular vector onto its original data field depicts the temporal variation of the singular vector. The correlation of the expansion coefficients between the two vectors evaluates the closeness of the two singular vectors (Wallace et al. 1992). These features make SVD a powerful and appropriate tool for the statistical intercomparison of two distinct fields.

3. Coupled intraseasonal variability between the ISM and the midlatitude circulation

Our analysis began with an examination of the standard deviations of intraseasonal variations at the 200-hPa geopotential height. The largest standard deviation is found in the exit region of the Atlantic jet stream over the northeastern Atlantic (Fig. 1a). This region also has the largest interannual variations (Ding and Wang 2005). The large variability of OLR (standard deviation >30 W m^{-2}) over the ISM domain is observed in the Bay of Bengal and offshore of the west coast of the Indian peninsula (Fig. 1b). In general, regions of large variability in convection coincide with regions of large long-term average values. Over the Indian peninsula, and particularly over northwestern India to the south of the Tibetan Plateau, the summer mean precipitation is high, and thus the intensity of ISO activity is comparable to that observed over the Indian Ocean with a value exceeding 25 W m^{-2}.

a. SVD mode between the midlatitude 200-hPa height and the ISM

To objectively search for the optimum midlatitude–ISM coupled pattern, we confined our SVD analysis to the ISM region (0°–30°N, 50°–100°E) for OLR (shown by the box in Fig. 1b) and to the Eurasian continent region (25°–72.5°N, 15°W–145°E) for 200-hPa geopo-

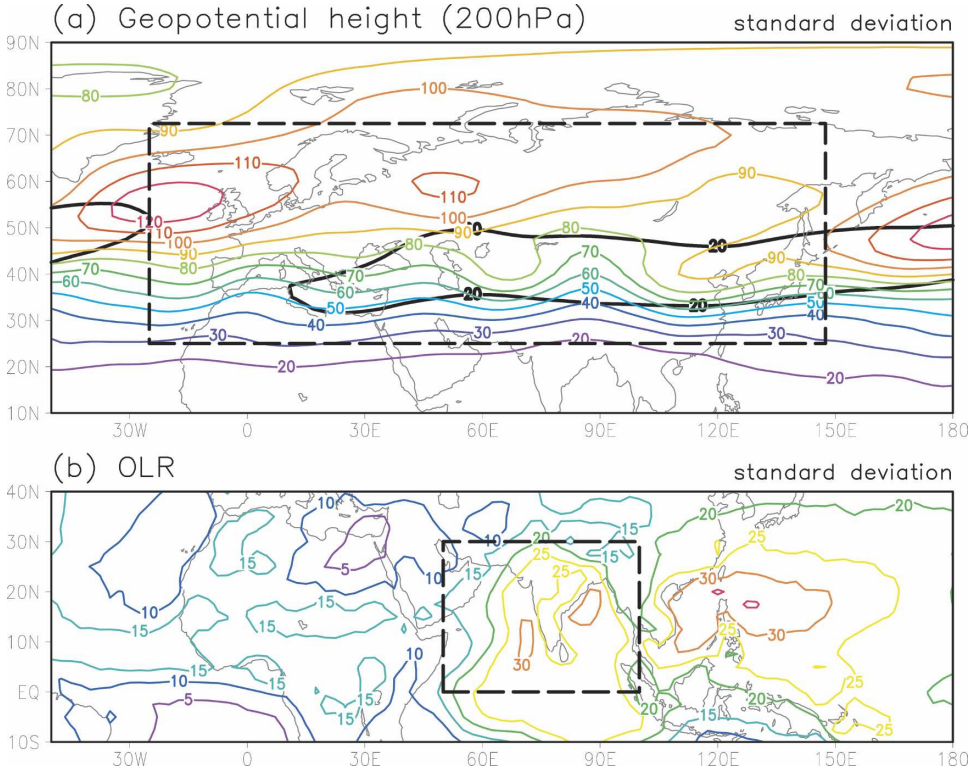

FIG. 1. Std dev of 25 summer daily (a) geopotential heights at 200 hPa (color contours every 10 m) and (b) OLR fields (color contours every 5 W m^{-2}). Climatological seasonal mean (June–September) zonal flow at 200 hPa (black contour above 20 m s^{-1}) is shown in (a). The domains for SVD analysis are denoted by dashed lines.

tential height (shown by the box in Fig. 1a). A square root of the latitudinal cosine weighting factor was used to compute the covariance matrix. The SVD analyses used both the normalized and unnormalized data, and no significant difference was found. We also compared the singular vectors to the heterogeneous regression maps and found that the two patterns are very similar to each other. Hereafter, we display the singular vectors of the temporal cross-covariance matrix between the normalized 25-summer daily heights and the OLR for the period from 1979 to 2003.

Figure 2 shows the leading SVD mode for geopotential heights and OLR. The square covariance fraction is 43.8%. Since the SCFs of the succeeding singular vectors are small (all below 15%), we focused our analysis on the first SVD modes. The height pattern (Fig. 2a) shows a wavelike pattern with positive anomalies over central Europe, central Asia, and northeastern Asia. Negative anomalies are found in the northeastern Atlantic and the western Siberia plain. Concurring with this height pattern, the OLR showed negative values in the whole ISM domain (Fig. 2b), suggesting that convection and precipitation over the entire ISM region are enhanced, especially over northern India, Pakistan, and the Arabian Sea. For simplicity, this region is termed the Northern Indian Summer Monsoon (NISM) region. A relatively high correlation coefficient (0.53) between the expansion coefficients of the two vectors indicates a close relationship between the two patterns, and in particular the association of the 200-hPa ridge over central Asia with the positive rainfall anomaly to its south.

Because of the strong seasonality of the midlatitude basic flow and the ISM, the SVD analysis was also performed for each month (June–September). The results are very similar (figures not shown) to the coupled modes for the entire summer season (Fig. 2). The midlatitude-ISM covarying pattern is thus robust throughout the Northern Hemisphere's summer.

b. *The vertical structure of the wave train and associated precipitation anomalies*

To understand the dynamics, we are concerned with the vertical structure of the midlatitude wave train and its possible role in linking the India rainfall oscillation with rainfall variability in remote areas. We calculated

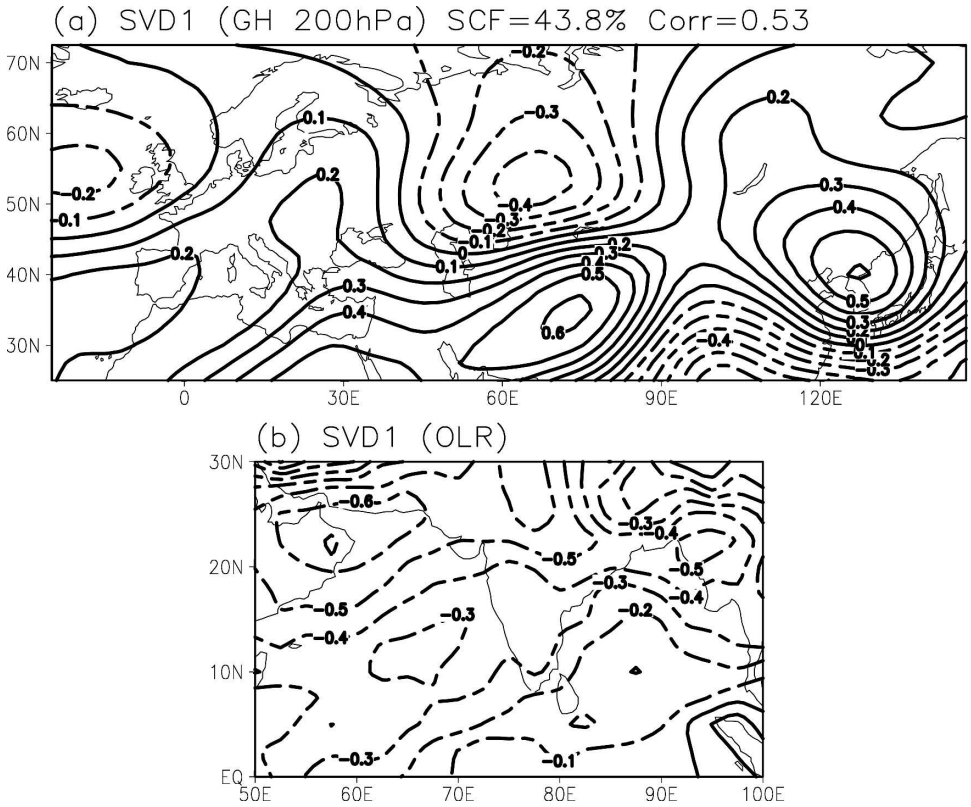

FIG. 2. Singular vectors of the first SVD mode for (a) geopotential heights at 200 hPa (contour interval of 0.1) and (b) OLR (contour interval of 0.1). SCF, expressed as a percentage and the temporal correlation coefficient between two expansion coefficients (Corr) are listed in (a). The SVD vectors are nondimensional.

the correlation coefficients of the expansion coefficient of SVD1 height with 700-hPa daily height and GPCP daily rainfall, respectively. The results are presented in Fig. 3. The correlated 700-hPa geopotential height anomalies resemble the pattern in the 200 hPa (Fig. 2a): an anomalous high over central Europe, a low over the western Siberia plain, and a major high anomaly over northeastern Asia. Thus, the wave train has an equiva-

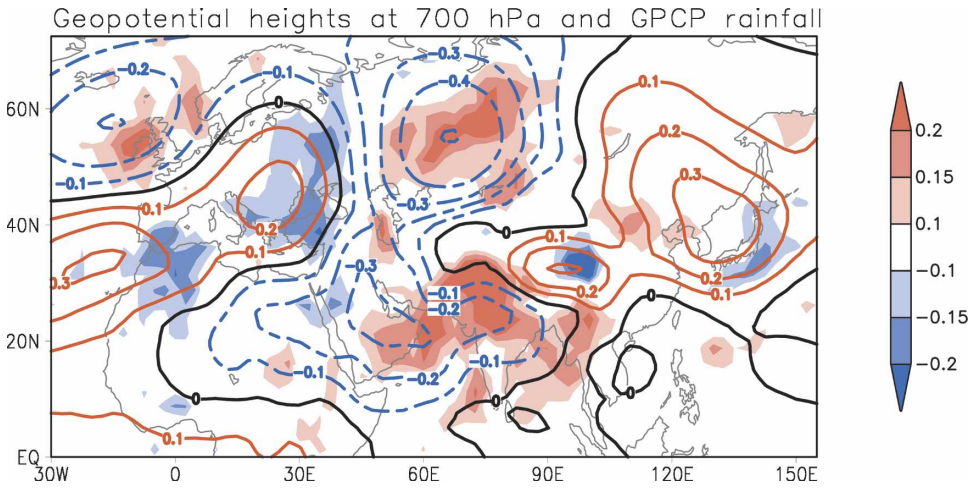

FIG. 3. Correlation coefficient between the expansion coefficient of the first SVD height mode (shown in Fig. 2a) and 25 summer daily 700-hPa heights (contour interval of 0.1) and GPCP rainfall (shading interval of 0.05) anomalies.

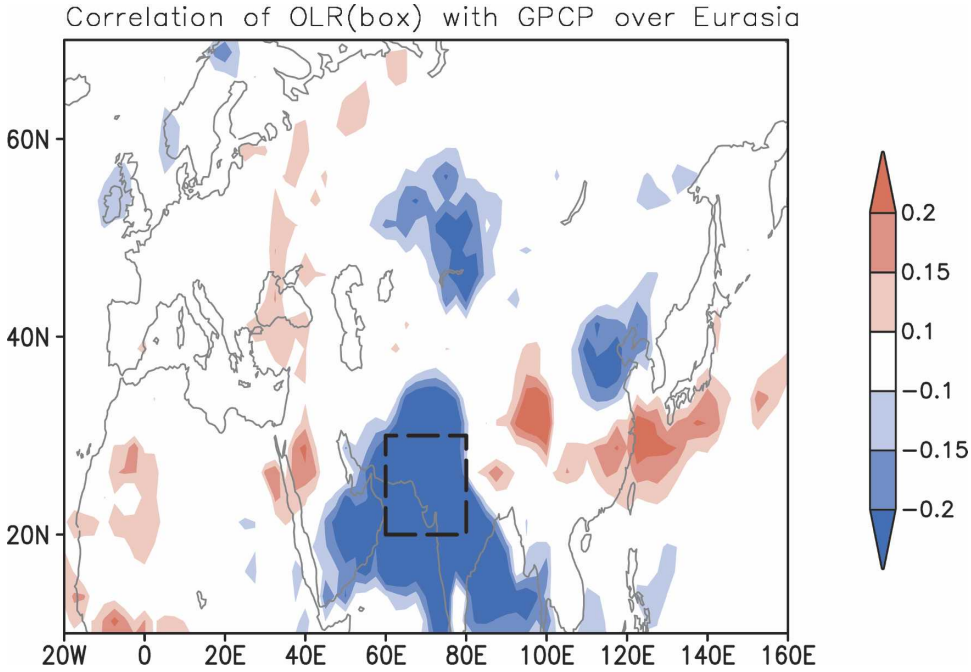

FIG. 4. Correlation coefficient between the time series of domain-averaged OLR over the NISM (shown as box) and 25 summer daily GPCP anomalies at each grid point over Eurasia (shading interval of 0.05).

lent barotropic structure in the midlatitudes. An exception is that the 200-hPa anomalous high over central Asia displays a tilted baroclinic structure, with a 700-hPa anomalous low occurring over the Arabian Peninsula and the Arabian Sea.

The comparison of the precipitation pattern and the height pattern shown in Fig. 3 indicates that the midlatitude wave train extending from central Europe to East Asia plays a role in connecting the rainfall anomalies along its path. The ISM has an in-phase teleconnection with the rainfall anomalies over northwestern Europe, the western Siberia plain, and north China, but an out-of-phase teleconnection with the rainfall anomalies over the eastern Mediterranean and Japan. The linkage between the northeastern Asian anomalous high and the dipole rainfall anomaly over East Asia can be explained by the moisture transport and convergence. The anomalous southeast wind to the west of the high increases atmospheric water vapor transport inland, and meanwhile, the anomalous northerly to the east of the high decreases water vapor transport. Thus, north China (middle reach of the Yellow River) receives above-normal precipitation, whereas Japan experiences drought conditions (Fig. 3). Note that the correlation between the area-averaged OLR over the NISM (20°–30°N, 60°–80°E) and GPCP rainfall over Eurasia are to some extent similar to the correlation of GPCP rainfall associated with the SVD1 height expansion coefficient, especially over north China (Fig. 4), suggesting that the in-phase teleconnection between the ISM and north China is robust. The lead–lag correlations between north China (35°–45°N, 110°–125°E) rainfall and NISM OLR (20°–30°N, 60°–80°E) were also calculated with a lead and lag up to 20 days. The most significant relationship was seen to occur at zero lag.

4. Origin and propagation of the intraseasonal Eurasian wave train

a. Time-lagged SVD analysis

Besides the simultaneous connections between the midlatitude wave train and the ISM, we are particularly concerned with the temporal phase relationship between the ISM and the midlatitude wave train. An attempt was made to determine the extent to which one system may lead another. For this purpose, we used the time-lagged SVD analysis (Czaja and Frankignoul 2002) to derive the lead–lag coupled patterns between the 25 summer daily geopotential height at 200 hPa (within Eurasia domain) and OLR within the ISM domain at a given lag ranging from −20 to +20 days. A total of 41 time lags were calculated and symbolized as SVD(−20), . . . , SVD(0), . . . , SVD(+20). For ex-

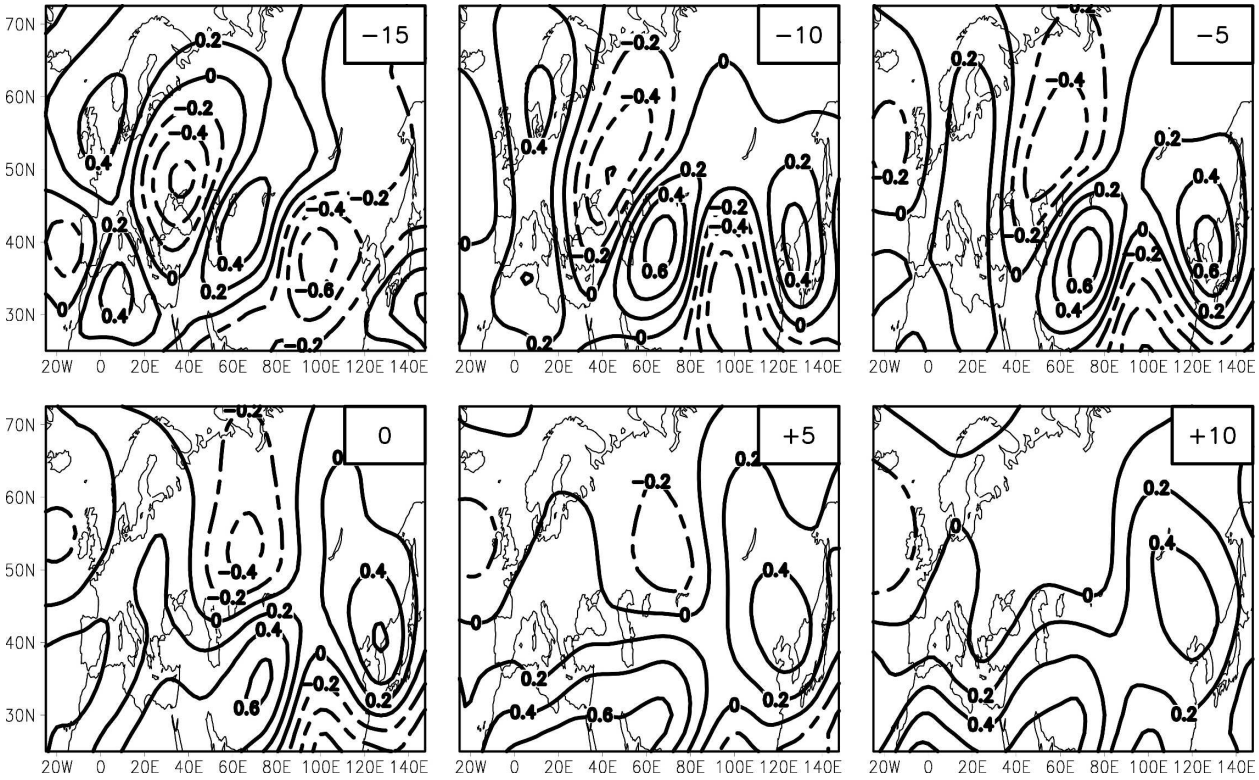

FIG. 5. Singular vectors of geopotential heights (contour interval of 0.2) for the first SVD mode between Eurasian 200-hPa heights and OLR anomalies over the ISM domain. The results are shown from day −15 to day +10. Lag days are indicated in the upper right-hand corner of each panel. The SVD vectors are nondimensional.

ample, SVD(−20) denotes a SVD analysis between the ISM OLR field and the midlatitude 200-hPa geopotential heights that lead OLR by 20 days. SVD(+20) is the same as SVD(−20) except that the OLR field leads the height field by 20 days. This objective method can capture the most favorable lead–lag relationship between the midlatitude circulation and the ISM convection. For each lag condition (from −20 to +20 days), the leading mode of time-lagged SVD analysis occupies a significant portion of the total squared covariance (above 35%), and the correlation coefficients between the expansion coefficients remain above 0.4. It is well justified, then, to focus on the first mode of the time-lagged SVD as representative of the dominant patterns of tropical–extratropical coupling.

It is noted that the OLR patterns at each time lag (from −20 to +20 days) have strikingly similar spatial and temporal characteristics to the OLR pattern at zero lag, which is already shown in Fig. 2b. The strong convection is in the entire ISM domain with a maximum convection located in the northwest part of the domain. Since this OLR pattern is strongly coupled with a midlatitude wave train across Eurasia (shown in Fig. 2a), the variations of the SVD geopotential height pattern from negative to positive lags (Fig. 5) describe the time evolution of the midlatitude wave train from a stage prior to the outbreak of the NISM convection to a stage after the outbreak.

At day −15 (the height precedes the OLR by 15 days), a wave train with alternating high and low pressure extends from the northeastern Atlantic to the area south of Japan. The strongest anomaly is seen in the Ural Mountain low. At day −10, the wave train moves slightly eastward and becomes more compact. The largest anomaly occurs in the central Asian high. At the same time, a high anomaly emerges in northeastern Asia. By day −5, the wave train is similar to that of day −10, but the strongest anomaly shifts farther downstream to both the central Asian high and the northeast Asian high. This pattern continues to the zero lag day, but the anomalies upstream of the central Asian high start to weaken. The entire sequence indicates an eastward and southward propagation of the energy along the Eurasian wave train. From day 0 to day +10, the central Asian high disperses southwestward, forming a ridge extending from northern India to North Africa. Meanwhile, the northeastern Asian high remains.

In addition, the time-lagged SVD analysis between

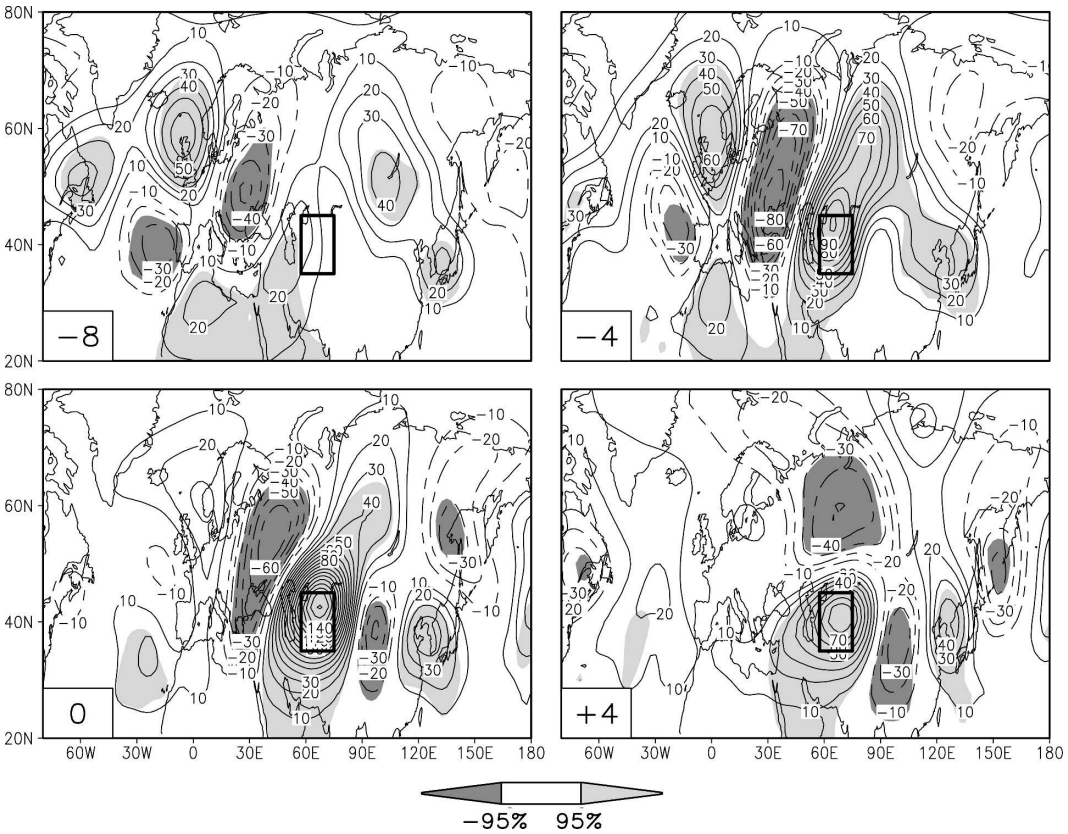

FIG. 6. Time sequence of the composite 200-hPa geopotential height anomalies (contour interval of 10 m) from day −8 to day +4 with respect to the maximum central Asian high, which occurs on day 0. The shading represents the anomalies that are significantly different from zero above the 95% level based on a simple *t* test. The rectangular box denotes the reference domain for the central Asian high.

OLR over the ISM domain and 500-hPa geopotential height over Eurasia reveals a similar evolution. These results show evidence that the large-scale midlatitude wave train leads the strong convection anomalies over the NISM region. The wave train emanating from the northeastern Atlantic to East Asia emerges 10–15 days prior to the outbreak of the convection over the NISM region. The general picture is that a quasi-stationary wave train propagates eastward and equatorward from the northeastern Atlantic into central Asia to establish an anomalous high from day −10 to day −5. Then, the wave train travels quickly eastward along the jet stream to amplify another anomalous high over northeastern Asia from day −5 to the zero lag day. The whole wave train pattern across Eurasia is well established before the outbreak of ISM convection, suggesting the possible role of the anomalous high over central Asia in triggering the strong convection over the NISM. Because the two anomalous highs of the midlatitude wave train are almost simultaneously established over central Asia and northeastern Asia, respectively, rainfall variations over the NISM occur nearly concurrently with the anomalous rainfall over north China (see section 3b).

b. Result of composite analyses

In this coupled mode, the anomalous high over central Asia associated with the midlatitude wave train precedes the strong convection over the NISM. It is conceivable that the central Asian high may trigger active convection over the NISM region. To identify signals associated with the extreme values of the anomalous high over central Asia, we performed a composite analysis based on the 200-hPa geopotential heights averaged in the following reference region: 35°–45°N, 55°–75°E (shown by the rectangular box in Fig. 6). A total of 28 extreme events were selected for the summers during the 1979–2003 period. Day 0 denotes the day on which the maximum anomalous high occurred over the reference region. The time sequence of the composite geopotential height from day −8 to day +4 (with a 4-day interval) is illustrated in Fig. 6. From day −8 to day −4, there is clear evidence of a wave train

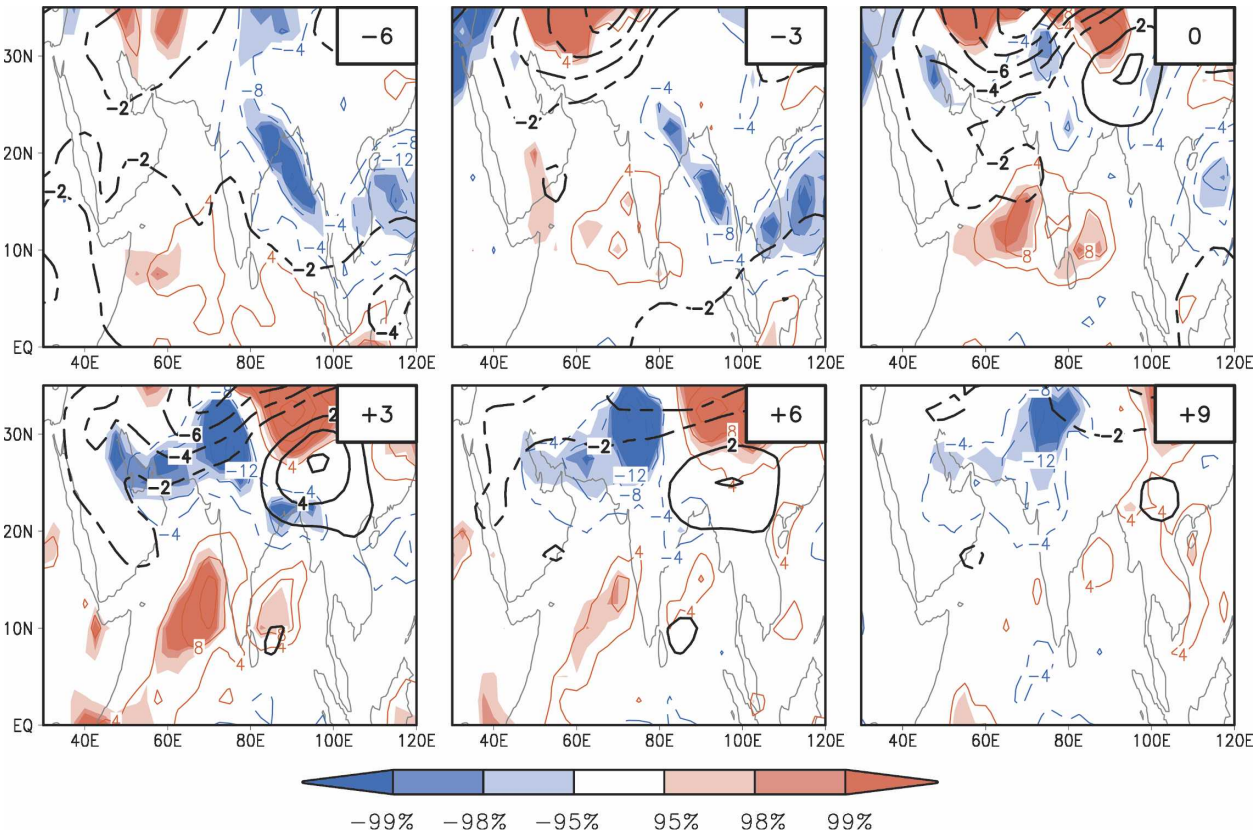

FIG. 7. Composite of OLR anomalies (color contour interval of 4 W m^{-2}) with respect to the same day 0 reference used in Fig. 6. The color shading represents the confidence level based on a simple *t* test. The black contours denote the zonal wind shear anomalies between 200 and 700 hPa (U200 − U700; contour interval of 2 m s^{-1}).

approaching central Asia from the northeastern Atlantic. As the significant upper-level anomalous high is established over the northeastern Atlantic, the wave train emanates eastward and splits into two branches. One turns equatorward, forming cyclonic and anticyclonic anomalies over the western Siberia plain and central Asia, respectively. Meanwhile, a secondary ray path is seen downstream along 60°N across northern Russia and reaching the Sea of Okhotsk. On day 0, the height anomaly over central Asia reaches its maximum intensity; the wave train continues migrating farther eastward to strengthen the anomalous ridge over northeastern Asia. After the anomalous high approaches its peak in central Asia, it quickly retreats westward (day +4).

The composite OLR anomalies that correspond to the same zero reference day of all 28 events are shown in Fig. 7. From day +3 to day +9, and even to day +15 (figure not shown), strong anomalous convection with anomalous OLR exceeding 10 W m^{-2} is seen over the NISM. The composite GPCP precipitation data yield a similar picture with the rainfall anomalies over northern India reaching 2–3 mm day^{-1} (figure not shown). Thus, over northern India, the duration of the active phase of the monsoon, induced by the upper-level high to the north, can last 10–15 days and produce about 30 mm of anomalous rainfall over the NISM area. Simple composite methods in terms of the anomalous high over central Asia appear to capture the essence of the whole coupled mode between the Eurasian wave train and NISM convection, indicating the vital role of the central Asian high in this tropical–extratropical interactive system.

5. Recurrent intraseasonal mode in the midlatitude circulation and the ISM

a. EOFs of the midlatitude circulation

While the spatial–temporal linkage between the midlatitude wave train and the ISM is well described by the lagged SVD and composite analysis, it is not clear whether the identified coupled patterns are statistically significant intraseasonal fluctuations in the respective fields. To answer this question, we applied EOF analy-

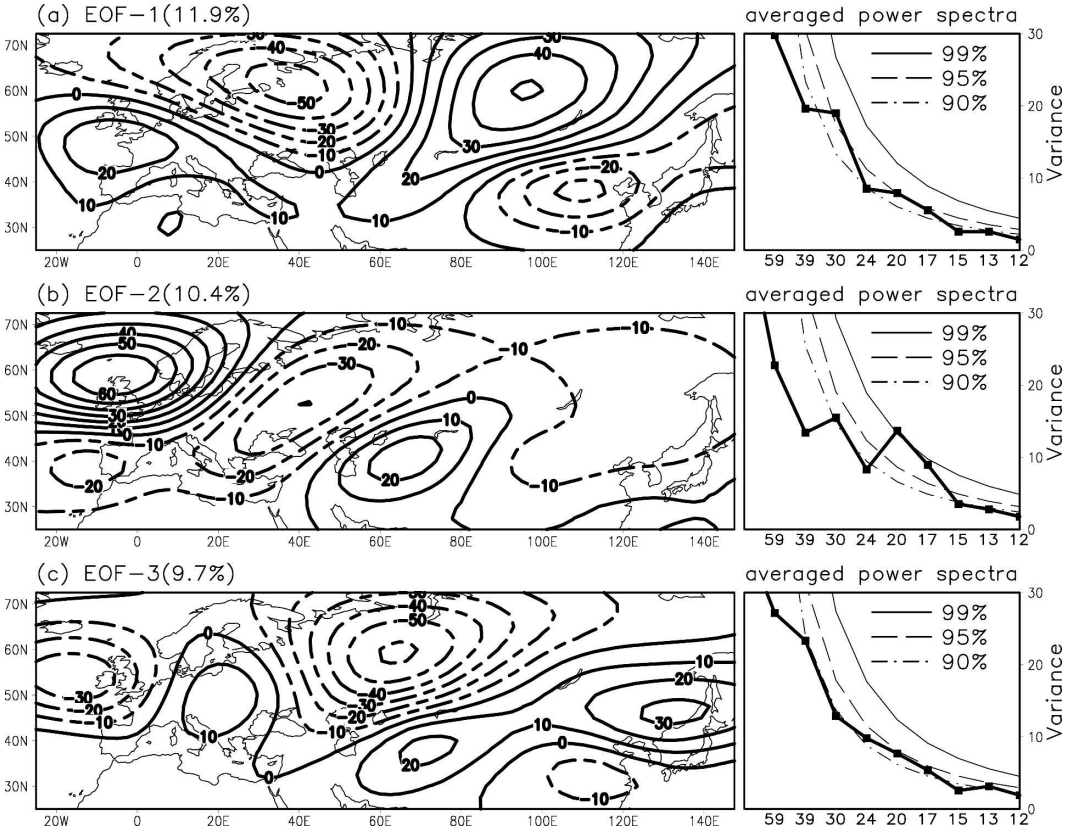

FIG. 8. (top to bottom) (left) First 3 EOF modes for 25 summer daily geopotential heights at 200 hPa (contour interval of 10 m) and (right) averaged normalized power spectrum of the corresponding PC as a function of the frequency in day^{-1}(thick line). The three EOF modes have been scaled by 1 std dev of the corresponding time series to give a unit of m; they occupy (a) 11.9%, (b) 10.4%, and (c) 9.7% of the total variance. Thin lines in the right panels represent the upper confidence bounds of red noise at the 90%, 95%, and 99% levels, respectively.

sis separately to the midlatitude atmospheric circulation and the ISM OLR anomalies.

First, an EOF analysis was performed on the 25 summer (1979–2003) 200-hPa daily geopotential height anomalies within the same domain as that used in the SVD analysis. The data were weighted by a square root of the latitudinal cosine factor. Figure 8 shows the first 3 leading EOFs of the geopotential height field, which explain 11.9%, 10.4%, and 9.7% of the total variance, respectively. The first EOF displays a high-latitude wave train extending from the region of the anomalous high over western Europe centered at the Bay of Biscay, passing through northern Russia and down to East Asia and the western North Pacific. The second EOF depicts an eastward and equatorward wave train, starting from an intense center of action over the northeastern Atlantic, centered at the northern tip of Scotland, and propagating from this action center to East Asia via the western Siberia plain and central Asia. It has features in common with those of the SVD1 height mode in day −15 [SVD(−15) in Fig. 5]. The most conspicuous feature of the third mode is a wave train consisting of three anomalous highs over central Europe, central Asia, and northeastern Asia and two anomalous lows over the northeastern Atlantic and the western Siberia plain. This wave train pattern is very similar to the SVD1 height pattern revealed in day −5 [SVD(−5) in Fig. 5], except for a northeastward shift of the anomalous northeastern Asian high.

The temporal and pattern correlation coefficients between the EOF2/EOF3 mode and the SVD1 height modes at each lag were calculated. For EOF2, both spatial and temporal correlations approach maxima at the lag of −14 days; the temporal correlation coefficient is 0.69, and the spatial correlation coefficient is 0.59. For EOF3, both the spatial and temporal correlations have maxima at the lag of −6 days; the temporal correlation coefficient is 0.80, and the spatial correlation coefficient is 0.75. It is indicated that the EOF2 and EOF3 of the 200-hPa geopotential height capture the different evolutionary phases of the midlatitude wave train prior to the outbreak of strong convection over

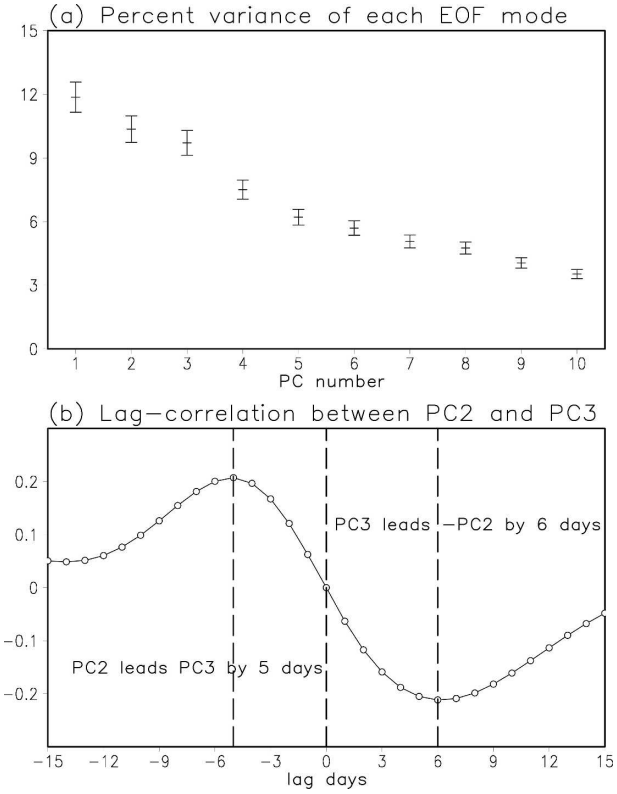

FIG. 9. (a) EOFs' structure for intraseasonal 200-hPa geopotential height anomalies in terms of the percent total variance explained by each EOF for their respective intraseasonal time series (first 3 EOFs shown in Fig. 8). Error bars were determined by the formula of North et al. (1982). (b) Lagged cross correlation between PCs of EOF2 and EOF3. A lag correlation with a negative lag day indicates that PC2 leads PC3. A lag correlation with a positive lag day indicates that PC3 leads PC2.

the NISM. The establishment of the anomalous wave train emanating from the northeastern Atlantic to East Asia can be used as an intraseasonal predictor for an active monsoon over the NISM.

The rule of North et al. (1982) was adopted to check whether the difference between a given eigenvalue and a neighboring eigenvalue is larger than the sampling error of the given eigenvalue. The calculation of the sampling error uses the degrees of freedom (450) that have removed the effect of autocorrelation. The results indicate that the first EOF was separated from the other EOF modes (Fig. 9a). However, the second and third EOFs are not separable, but both are well distinguished from the rest of the EOFs. Figure 9b shows the lag correlation coefficients between the principal components (PCs) of EOF2 and EOF3. The maximum lagging correlation occurs when the PC2 leads PC3 by 6 days, and PC3 leads the negative of PC2 by 5 days, indicating a period of around 20 days of oscillation. Thus, EOF2 and EOF3 can be considered "twin modes" of the midlatitude intraseasonal variability. Together, EOF2 and EOF3 account for about 20% of the intraseasonal variance within the domain and reflect a midlatitude ISO including an eastward and equatorward propagation of a Rossby wave train from the northeastern Atlantic to East Asia. Given the moderate magnitude of the maximum lag correlation between two PCs, the oscillating behavior of the twin modes (EOF2 and EOF3) is not very stable and may be disrupted by the strong disturbance over the midlatitude.

The period of the wave train oscillation is determined by the spectral analysis of the first three PCs using NCAR Command Language software. Normalized spectra derived for each summer were averaged over the 25 yr to form averaged spectra, which are presented in the right-hand side of Fig. 8. PC1 shows a spectrum with a statistically significant peak centered at 30 days at the 95% confidence level against a red noise process, while PC2 is dominated by a relative shorter period of 20 days at the 99% confidence level. The period of PC3 is modulated by 2 spectrum peaks at 20 days and 13 days at nearly the 95% confidence level. One has to be cautious about the significance of the averaged power spectra peak, however, because of the large interannual variation of power spectrum. Indeed, during the 25 yr from 1979 to 2003, the 20-day period of PC2 is significant (above the 95% confidence level) in 18 yr, and the 20-day period of PC3 is significant (above the 90% confidence level) in 17 yr. Thus, the dominant period of midlatitude ISO revealed in twin modes does not prevail in each summer. It may vary in its time band in some years.

b. EOFs of the ISM OLR

Additionally, the first two leading EOF modes of OLR in the ISM domain and the corresponding averaged power spectra are presented in Fig. 10. Note that the two leading EOFs together describe a well-organized northward propagation of convection anomalies, from the equatorial Indian Ocean toward the Indian subcontinent, that agree well with the previous results (e.g., Lau and Chan 1986; Lawrence and Webster 2001; Jiang and Li 2005). The maximum correlation between 2 PCs is 0.36 at a 7–8-day lag, confirming the dominant spectra peak of 2 modes at 30–40 days (right-hand side of Fig. 10). The EOF2 of OLR, which explains about 14.7% of the intraseasonal variance within the domain, bears close resemblance to the typical active/break phase of the ISM (Krishnan et al. 2000; Goswami 2005). Both the spatial correlation coefficient (0.63) and the temporal correlation coefficient (0.54) show robust coherence between this EOF2 mode and the OLR pattern in SVD analysis (Fig. 2b). Thus,

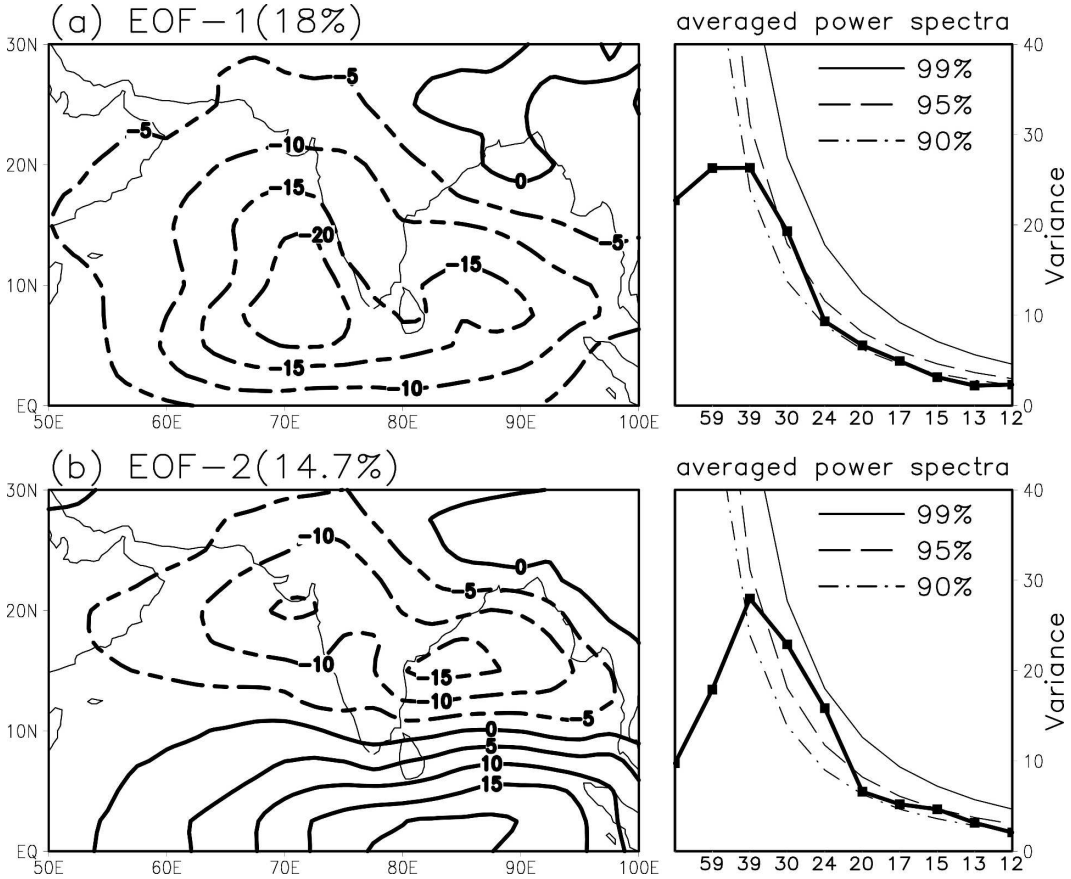

FIG. 10. (top to bottom) (left) First 2 EOF modes for 25 summer daily OLR at the ISM domain (contour interval of 5 W m^{-2}) and (right) averaged normalized power spectrum of the corresponding PC as a function of the frequency in day^{-1}(thick line). The 2 EOF modes have been scaled by one std dev of the corresponding time series to give a unit of W m^{-2}; they occupy (a) 18% and (b) 14.7% of the total variance. Thin lines in the right panels represent the upper confidence bounds of red noise at the 90%, 95%, and 99% levels, respectively.

the midlatitude wave train tends to precede the active/break phase of the NISM.

The results of EOF analysis corroborate the finding of the SVD analysis and reveal that the recurrent oscillation modes of midlatitude circulation and the typical active/break phase of the NISM convection are coupled together to form a significant midlatitude ISM connection. The analysis also indicates that the active/break phase of the ISM is not only influenced by the systems originating from the equatorial region (EOF1 of OLR) but is also affected to some extent by the activity of the midlatitude ISO.

6. Discussion

a. Origin and propagation of the intraseasonal wave train

The results presented in sections 4 and 5 suggest that the intraseasonal variability over the northeastern Atlantic is important for understanding the origin of the midlatitude wave train. What gives rise to the intraseasonal oscillation in the northeastern Atlantic jet stream exit region? According to Simmons et al. (1983), the disturbances in the jet stream exit region can be readily excited by tropical forcing through barotropic energy conversions associated with both the meridional and zonal gradients of the basic flow. The zonal gradients of the basic flow are particularly strong in the jet stream exit region. It is possible that the strong intraseasonal variance of upper-tropospheric circulation over the northeastern Atlantic in the exit region of the Atlantic jet stream (Fig. 1a) is associated with the barotropic instability of the summer mean flow. The northeastern Atlantic anomalous high, which can be considered the origin of the midlatitude wave train, is presumably excited by efficient kinetic energy extraction from the basic state. The upstream tropical or extratopical forcing along the jet stream can frequently excite this initial cell

of the midlatitude wave train over the northeastern Atlantic.

Barotropic modeling by Branstator (1983) shows that zonal variations of the winter mean flow tend to enhance the equatorward propagation of Rossby waves in a large-scale pressure ridge. Because the Tibetan Plateau acts as a heat source in northern summer, a prominent large-scale ridge over the Caspian Sea is an important feature of the climatological basic flow in the upper troposphere. The upper-tropospheric zonal flow over the Caspian Sea also contains marked longitudinal variation (figures not shown). Accordingly, it is rational to expect that the combination of the zonal variation of zonal wind and the large-scale ridge over the Caspian Sea could favor the equatorward propagation of a Rossby wave train. Namely, the wave propagation originating from the northeastern Atlantic tends to yield an arch-shaped wave train that migrates from the northeastern Atlantic to central Asia via the western Siberia plain. Two factors, namely, the strong barotropic instability at the exit region of the Atlantic jet stream and the large-scale ridge over the Caspian Sea, may be instrumental in understanding the initiation and propagation of the midlatitude wave train.

b. Positive feedback between the midlatitude wave train and the NISM

The above results have shown evidence of a robust connection between the summer monsoon activity over the NISM region and the upper-level anomalous high over central Asia. However, the actual mechanism of this linkage remains elusive. In particular, it is unknown how the anomalous high over central Asia modifies rainfall variability over the NISM. The answer to this question is one of the keys to understanding the intraseasonal interaction between the ISM and midlatitude systems.

One possible explanation is the role of the easterly vertical shear. To the south of the central Asian anomalous high, the easterly anomalies in the upper troposphere reinforce an easterly vertical shear over northern India. Previous theoretical work suggested that an easterly vertical shear alone can destabilize equatorial Rossby waves by feeding mean flow available potential energy to the waves (Moorthi and Arakawa 1985; Wang 1990). In the presence of the boundary layer, the moist Rossby wave instability is remarkably enhanced by easterly vertical shear and suppressed by westerly vertical shear (Xie and Wang 1996). The reason is that an easterly vertical shear over northern India may confine the Rossby wave response to the lower levels (Wang and Xie 1996). This will produce a strong interaction between the Rossby wave and the boundary layer Ekman-pumping-induced condensation heating. This increased easterly vertical shear also generates an enhanced meridional heat flux that favors the conversion of mean flow available potential energy to eddy available potential energy. Both effects would increase equatorial Rossby wave instability in the atmosphere by providing wave available potential energy, thereby increasing monsoon precipitation. It is clear from Fig. 7 that enhanced easterly vertical shear (U200 minus U700) anomalies to the south of the anomalous high occur prior to the peaks of convection anomalies over the NISM. Lead–lag correlations between the local easterly vertical shear and OLR anomalies over the NISM demonstrate that the vertical shear tends to precede rainfall anomalies by 2–4 days (figure not shown). Therefore, the enhanced central Asian high may lead to enhanced precipitation in the NISM region by strengthening the easterly vertical shear.

Another possible dynamic interpretation is that the strengthened easterly jet stream to the south of the upper-tropospheric anomalous high may induce a northerly ageostrophic flow and, as a result, generate the upper-level divergence and strong upward motion over the NISM (Hoskins and Wang 2005). However, in the composite of vertical motion for the same 28 extreme events (figures not shown), pronounced upward motion and convection anomalies over the NISM occurred almost simultaneously. It seems that the causality between these two factors is not easily diagnosable through observational analyses.

Because the enhanced convection over the NISM region is associated with the baroclinic structure of the local circulation anomaly (Fig. 3), we suggest that after the strong convection is excited by the anomalous central Asian high, the resulting diabatic heating may likely induce a baroclinic Rossby wave response to the west of the heating source (Gill 1980; Rodwell and Hoskins 1996). The westward retreat of the central Asian high after its establishment can be taken as a hint of the Rossby wave response to the ISM heating. Hoskins and Ambrizzi (1993) suggested that on the left side of the local anticyclonic anomaly induced by the heat source over India, the low-vorticity air is advected from the south, producing a vorticity anomaly to enhance the existing local vorticity. Hence, an upstream extension of the forced anomaly is generated, and the induced circulation is drastically broader than the forced anomaly. This mechanism is particularly effective when the jet stream core coincides with the center of the initial forced anomalous high.

A positive feedback between the rainfall anomalies and moisture transport may also be important for the maintenance of the strong convection over the NISM.

The strengthened rainfall anomalies over northern India lead to an anomalous low over the Arabian Sea at low levels via Rossby wave dispersion. This cyclonic circulation (Fig. 3) that impinges on the southern flank of the Tibetan Plateau may carry more moisture to the NISM and strengthen the deep convection and rainfall activity there.

Based on the above speculations, we propose a positive interaction between the anomalous high over central Asia and strong convection over the northern ISM region. Strong convection over the northern ISM region is initially triggered by the anomalous central Asian high within the westerly wave train extending from the northeastern Atlantic to East Asia (Fig. 11a). Conversely, the convection is likely to excite a Rossby wave response, which reinforces the central Asian high. Because this high is embedded in the westerly jet stream, the Rossby wave energy dispersion associated with the central Asian high may enhance the downstream circulation anomalies over northeastern Asia (Fig. 11b). In the time-lagged SVD analysis (Fig. 5), the maintenance of the anomalous high over northeastern Asia after an active phase of the NISM may suggest this effect.

7. Summary and concluding remarks

a. Summary

This study shows how the "active" and "break" phases of the ISM are altered by the midlatitude systems on an intraseasonal time scale. The SVD analysis was utilized to identify the most dominant mode of covariation between the upper-tropospheric geopotential height over Eurasia and the convection (implied by OLR) over the ISM region. The leading SVD modes explain 43.8% of the covariability, and the correlation coefficient between the two expansion coefficients approaches 0.53. The first SVD mode reveals a strong relationship between enhanced convection over northern India, Pakistan, and the Arabian Sea and a midlatitude wave train pattern spanning Eurasia, with prominent highs over central Europe, central Asia, and northeastern Asia and a low over the western Siberia plain. The time-lagged SVD analyses from the −20 day lag to the +20 day lag further show the eastward propagation of the midlatitude wave train and the role of this wave train in initiating the convection anomalies over the NISM.

The essence of intraseasonal midlatitude ISM interaction is captured by the composites of the 28 strongest anomalous central Asian high events, since the enhanced convection over the northern ISM region could primarily arise from the direct forcing of this high.

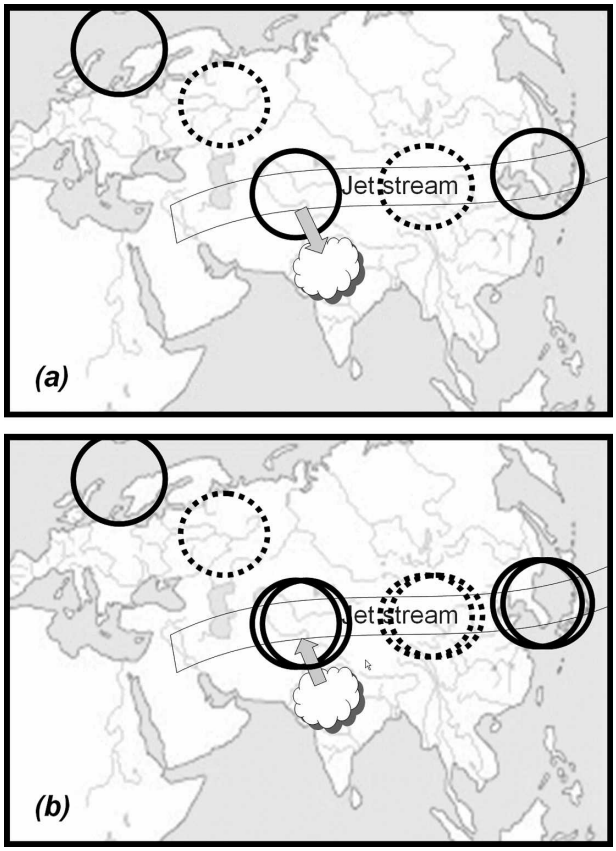

FIG. 11. To visualize the hypothesis proposed in the discussion section, a schematic diagram is presented to illustrate the possible positive feedback between the Eurasian wave train and the ISM on an intraseasonal time scale. The cloud denotes the strong convection over the northern ISM region, and the circles represent the Eurasian wave train in the upper troposphere. The solid circle represents the anticyclonic circulation and the dashed circle denotes the cyclonic circulation. (a) The strong convection over the northern ISM region is initially triggered by the anomalous central Asian high within the wave train extending from the northeastern Atlantic to East Asia, and then (b) the convection, in turn, excites a Rossby wave response to reinforce the central Asian high and downstream circulation anomalies of the wave train, through Rossby wave dispersion.

EOF analysis is further used to detect the spatiotemporal structure of the dominant intraseasonal variations that are recurrent in the OLR and midlatitude height field, respectively. The EOF2 mode of the OLR field accounting for 14.7% variance represents the typical active/break phase of the ISM and bears close similarity to the OLR pattern in the SVD analysis. The second and third EOF modes of 200-hPa geopotential heights are together distinguished from other modes, and they explain 20% of the total intraseasonal height variance. These "twin modes" represent a 20-day midlatitude ISO extending from the Atlantic to East Asia, and they capture different propagating phases of the wave train

pattern revealed by time-lagged SVD analysis. It is concluded that the recurrent modes of midlatitude circulation and the ISM are coupled together to form the dominant midlatitude ISM connection.

The picture emerging from the SVD, EOF, and composite analyses suggests that an anomalous high appears to occur initially in the northeastern Atlantic, forming a Rossby wave train that propagates eastward toward central Asia and then travels farther to East Asia and the West Pacific along the westerly jet stream. The vertical structure of this wave train presents a considerable barotropic component, except that the central Asian anomalous high exhibits a baroclinic character.

Once the anomalous high is generated over central Asia, it can excite convection over the northern ISM region. Afterward, it quickly retreats westward. Meanwhile, the anomalous high over northeast Asia induces increased rainfall over north China and decreased rainfall over Japan. On an intraseasonal time scale, the midlatitude wave train establishes a teleconnection of strong NISM concurrent with above-normal rainfall over northwestern Europe, the western Siberia plain, and north China, and below-normal rainfall over the eastern Mediterranean and Japan.

We note that the "monsoon–desert" mechanism proposed by Hoskins and Rodwell (1995) and Rodwell and Hoskins (1996) can be used to explain the out-of-phase relationship in rainfall variability between the ISM region and the eastern Mediterranean (Figs. 3, 4). In addition, the passage of midlatitude wave trains over Eurasia may be another explanation for this out-of-phase relationship.

It is not immediately clear what effect the anomalous central Asian high has on the convection over the northern ISM region. This cannot be assessed solely based on observation. We speculate that convection is enhanced by the increased easterly vertical shear. The clue for such a possibility is provided by the lead–lag correlation between easterly vertical shear and OLR over the northern ISM region. The correlation shows that the easterly vertical shear between 200 and 700 hPa leads local OLR anomalies by 2–4 days. The mechanisms that cause strong convection over the northern ISM region are hypothesized as follows: to the south of the anomalous central Asian high, the easterly anomalies in the upper troposphere strengthen the easterly vertical shear over the northern ISM region; this increased shear traps the Rossby wave in the lower troposphere, which enhances the convective interaction with dynamics through boundary layer convergence and increases the moist baroclinic instability, thereby increasing monsoon precipitation through the vertical shear mechanism proposed by Wang and Xie (1996) and Xie and Wang (1996).

Although the ISOs originating from the equator are very important rainfall-producing mechanisms for the intraseasonal variability of the ISM, the possible influence of the midlatitude flow on the intraseasonal variations in the NISM is suggested in this study. The monsoon intraseasonal oscillation in the NISM is influenced by disturbances from both the equator and the midlatitudes. Possibly, some rainfall events over India are caused by the interaction between the influences from the north and from the south.

b. Concluding remarks

The complexity of the interaction between the wave train and the ISM leaves several interesting problems for further studies. One area of interest is how the intraseasonal variability is generated in the northeastern Atlantic. Further studies are needed before a conclusion can be made concerning the cause of the linkage between the anomalous high over central Asia and intraseasonal variability of the ISM. The hypothesis advanced in this paper is qualitative and based primarily on the results derived from empirical analysis. Dynamic processes of the midlatitude ISM interaction should be examined quantitatively in the future.

On an interannual time scale, Ding and Wang (2005) documented a circumglobal teleconnection (CGT) pattern that is recurrent in the boreal summer in the northern extratropics and acts to induce global-scale rainfall and temperature anomaly patterns around the Northern Hemisphere, linking western Europe, European Russia, India, East Asia, and North America. Because the intraseasonal midlatitude wave train and interannual CGT are governed by a similar spatial mode over Eurasia, it would be worthwhile to examine the potential interaction between the intraseasonal wave train and the interannual variability of the CGT.

By using relatively long periods of observed daily circulation and convection data, we found unambiguous evidence that the midlatitude wave train over Eurasia partly determines the active and break conditions of the ISM over northern India/Pakistan. This result has important implications in monsoon prediction and simulation, as it suggests that midlatitude systems could have some influence on the intraseasonal oscillations of the Indian summer monsoon and the East Asian summer monsoon. Thus, the prediction of the Indian summer monsoon and the East Asian summer monsoon intraseasonal variations should take into account the interaction between the midlatitudes and the monsoon systems.

Acknowledgments. This study has been supported by National Science Foundation/Climate Dynamics Program Award ATM-0647995. The authors appreciate the anonymous reviewers' comments on an early version of the manuscript, which led to significant improvement. Thanks are also extended to Drs. S.-P. Xie, F. F. Jin, T. Li, S. Nicholson, and T. Dunn for fruitful discussions.

REFERENCES

Annamalai, H., and J. M. Slingo, 2001: Active/break cycles: Diagnosis of the intraseasonal variability of the Asian summer monsoon. *Climate Dyn.,* **18,** 85–102.

Branstator, G., 1983: Horizontal energy propagation in a barotropic atmosphere with meridional and zonal structure. *J. Atmos. Sci.,* **40,** 1689–1708.

Bretherton, C. S., C. Smith, and J. M. Wallace, 1992: An intercomparison of methods for finding coupled patterns in climate data. *J. Climate,* **5,** 541–560.

Chen, W.-Y., 1982: Fluctuations in Northern Hemisphere 700-mb height field associated with southern oscillation. *Mon. Wea. Rev.,* **110,** 808–832.

Czaja, A., and C. Frankignoul, 2002: Observed impact of Atlantic SST anomalies on the North Atlantic Oscillation. *J. Climate,* **15,** 606–623.

Ding, Q.-H., and B. Wang, 2005: Circumglobal teleconnection in the Northern Hemisphere summer. *J. Climate,* **18,** 3483–3505.

Ding, Y.-H., and D. R. Sikka, 2005: Synoptic systems and weather in the Asian monsoon. *The Asian Monsoon,* B. Wang, Ed., Springer Praxis, 131–201.

Fu, X.-H., B. Wang, T. Li, and J. McCreary, 2003: Coupling between northward-propagating, intraseasonal oscillations and sea surface temperature in the Indian Ocean. *J. Atmos. Sci.,* **60,** 1733–1753.

Fujinami, H., and T. Yasunari, 2004: Submonthly variability of convection and circulation over and around the Tibetan Plateau during the boreal summer. *J. Meteor. Soc. Japan,* **82,** 1545–1564.

Gill, A. E., 1980: Some simple solutions for heat induced tropical circulation. *Quart. J. Roy. Meteor. Soc.,* **106,** 447–462.

Goswami, B. N., 2005: South Asian monsoon. *Intraseasonal Variability of the Atmosphere-Ocean Climate System,* K. M. Lau and D. E. Waliser, Eds., Springer Praxis, 19–61.

——, and J. Shukla, 1984: Quasi-periodic oscillations in a symmetric general circulation model. *J. Atmos. Sci.,* **41,** 20–37.

Hartmann, D. L., and M. L. Michelson, 1989: Intraseasonal periodicities in Indian rainfall. *J. Atmos. Sci.,* **46,** 2838–2862.

Hoskins, B. J., and T. Ambrizzi, 1993: Rossby wave propagation on a realistic longitudinally varying flow. *J. Atmos. Sci.,* **50,** 1661–1671.

——, and M. J. Rodwell, 1995: A model of the Asian summer monsoon I: The global scale. *J. Atmos. Sci.,* **52,** 1329–1340.

——, and B. Wang, 2005: Large-scale atmospheric dynamics. *The Asian Monsoon,* B. Wang, Ed., Springer Praxis, 357–415.

Jiang, X.-A., and T. Li, 2005: Reinitiation of the boreal summer intraseasonal oscillation in the tropical Indian Ocean. *J. Climate,* **18,** 3777–3795.

——, ——, and B. Wang, 2004: Structures and mechanisms of the northward propagating boreal summer intraseasonal oscillation. *J. Climate,* **17,** 1022–1039.

Kemball-Cook, S., and B. Wang, 2001: Equatorial waves and air–sea interaction in the boreal summer intraseasonal oscillation. *J. Climate,* **14,** 2923–2942.

Keshavamurty, R. N., and M. S. Rao, 1992: *The Physics of Monsoons*. Allied, 199 pp.

Kripalani, R. H., A. Kulkarni, and S. V. Singh, 1997: Association of the Indian summer monsoon with the Northern Hemisphere mid-latitude circulation. *Int. J. Climatol.,* **17,** 1055–1067.

Krishnamurti, T. N., and H. N. Bhalme, 1976: Oscillations of a monsoon system. Part I. Observational aspects. *J. Atmos. Sci.,* **33,** 1937–1954.

——, and D. Subrahmanyam, 1982: The 30–50 day mode at 850 mb during MONEX. *J. Atmos. Sci.,* **39,** 2088–2095.

Krishnan, R., C. Zhang, and M. Sugi, 2000: Dynamics of breaks in the Indian summer monsoon. *J. Atmos. Sci.,* **57,** 1354–1372.

Lau, K.-M., and P. H. Chan, 1986: Aspects of the 40-50 day oscillation during the northern summer as inferred from outgoing longwave radiation. *Mon. Wea. Rev.,* **114,** 1354–1367.

Lawrence, D. M., and P. J. Webster, 2001: Interannual variations of the intraseasonal oscillation in the South Asian summer monsoon region. *J. Climate,* **14,** 2910–2922.

Liebmann, B., and C. A. Smith, 1996: Description of a complete (interpolated) OLR dataset. *Bull. Amer. Meteor. Soc.,* **77,** 1275–1277.

Livezey, R. E., and W.-Y. Chen, 1983: Statistical field significance and its determination by Monte Carlo techniques. *Mon. Wea. Rev.,* **111,** 46–59.

Moorthi, S., and A. Arakawa, 1985: Baroclinic instability with cumulus heating. *J. Atmos. Sci.,* **42,** 2007–2031.

Murakami, T., T. Nakazawa, and J. He, 1984: On the 40–50 day oscillation during 1979 Northern Hemisphere summer. Part 1: Phase propagation. *J. Meteor. Soc. Japan,* **62,** 440–468.

North, G. R., T. L. Bell, R. F. Cahalan, and F. J. Moeng, 1982: Sampling errors in the estimation of empirical orthogonal functions. *Mon. Wea. Rev.,* **110,** 699–706.

Raman, C. R. V., and Y. P. Rao, 1981: Blocking highs over Asia and monsoon droughts over India. *Nature,* **289,** 271–273.

Ramaswamy, C., 1962: Breaks in the Indian summer monsoon as a phenomenon of interaction between the easterly and the subtropical westerly jet streams. *Tellus,* **14A,** 337–349.

Rodwell, M. J., and B. J. Hoskins, 1996: Monsoons and the dynamics of deserts. *Quart. J. Roy. Meteor. Soc.,* **122,** 1385–1404.

Sikka, D. R., and S. Gadgil, 1980: On the maximum cloud zone and the ITCZ over Indian longitudes during the southwest monsoon. *Mon. Wea. Rev.,* **108,** 1840–1853.

Simmons, A. J., J. M. Wallace, and G. W. Branstator, 1983: Barotropic wave propagation and instability, and atmospheric teleconnection patterns. *J. Atmos. Sci.,* **40,** 1363–1392.

Tao, S.-Y., and L.-X. Chen, 1987: A review of recent research on the East Asian summer monsoon in China. *Monsoon Meteorology,* C. P. Chang and T. N. Krishnamurti, Eds., Oxford University Press, 60–92.

Wallace, J. M., C. Smith, and C. S. Bretherton, 1992: Singular value decomposition of wintertime sea surface temperature and 500-mb height anomalies. *J. Climate,* **5,** 561–576.

Wang, B., 1990: On the asymmetry of baroclinic instability between easterly and westerly shear. *Tellus,* **42A,** 463–468.

——, 2005: Theory. *Intraseasonal Variability of the Atmosphere-Ocean Climate System,* K. M. Lau and D. E. Waliser, Eds., Springer Praxis, 307–360.

——, and H.-L. Rui, 1990: Synoptic climatology of transient tropi-

cal intraseasonal convection anomalies: 1975–1985. *Meteor. Atmos. Phys.,* **44,** 43–61.

——, and X.-S. Xie, 1996: Low-frequency equatorial waves in vertically sheared zonal flow. Part I: Stable waves. *J. Atmos. Sci.,* **53,** 449–467.

——, and ——, 1997: A model for the boreal summer intraseasonal oscillation. *J. Atmos. Sci.,* **54,** 72–86.

——, R.-G. Wu, and K.-M. Lau, 2001: Interannual variability of the Asian summer monsoon: Contrasts between the Indian and the western North Pacific–East Asian monsoons. *J. Climate,* **14,** 4073–4090.

Webster, P. J., 1983: Mechanism of monsoon low-frequency variability: Surface hydrological effects. *J. Atmos. Sci.,* **40,** 2110–2124.

——, V. O. Magana, T. N. Palmer, J. Shukla, R. A. Tomas, M. Yanai, and T. Yasunari, 1998: The monsoon: Processes, predictability and the prospects for prediction. *J. Geophys. Res.,* **103,** 14 451–14 510.

Wilks, D. S., 1995: *Statistical Methods in the Atmospheric Sciences: An Introduction*. Academic Press, 467 pp.

Xie, X.-S., and B. Wang, 1996: Low-frequency equatorial waves in vertically sheared zonal flow. Part II: Unstable waves. *J. Atmos. Sci.,* **53,** 3589–3605.

Yasunari, T., 1979: Cloudiness fluctuation associated with the Northern Hemisphere summer monsoon. *J. Meteor. Soc. Japan,* **57,** 227–242.

——, 1980: A quasi-stationary appearance of 30–40 day period in the cloudiness fluctuation during summer monsoon over India. *J. Meteor. Soc. Japan,* **58,** 225–229.

——, 1986: Low-frequency interactions between the summer monsoon and the Northern Hemisphere westerlies. *J. Meteor. Soc. Japan,* **64,** 693–708.